Geochemistry Geophysics Geosystems G3
AN ELECTRONIC JOURNAL OF THE EARTH SCIENCES
Published by AGU and the Geochemical Society

Article
Volume 8, Number 8
21 August 2007
Q08010, doi:10.1029/2007GC001655
ISSN: 1525-2027

Surface wave tomography of the western United States from ambient seismic noise: Rayleigh wave group velocity maps

M. P. Moschetti and M. H. Ritzwoller
Center for Imaging the Earth's Interior, Department of Physics, University of Colorado at Boulder, Campus Box 390, Boulder, Colorado 80309, USA (morganm@ciei.colorado.edu)

N. M. Shapiro
Laboratoire de Sismologie, CNRS, IPGP, 4 place Jussieu, 75005 Paris, France

[1] We have applied ambient noise surface wave tomography to data that have emerged continuously from the EarthScope USArray Transportable Array (TA) between October 2004 and January 2007. Estimated Green's functions result by cross-correlating noise records between every station-pair in the network. The 340 stations yield a total of more than 55,000 interstation paths. Within the 5- to 50-s period band, we measure the dispersion characteristics of Rayleigh waves using frequency-time analysis. High-resolution group velocity maps at 8-, 16-, 24-, 30-, and 40-s periods are presented for the western United States. The footprint of the TA encloses a region with a resolution of about the average interstation spacing (~70 km). Velocity anomalies in the group velocity maps correlate well with the dominant geological features of the western United States. Coherent velocity anomalies are associated with the Sierra Nevada, Peninsular, and Cascade Ranges, Great Valley, Salton Trough, and Columbia basins, the Columbia River flood basalts, the Snake River Plain and Yellowstone, and mantle wedge features associated with the subducting Juan de Fuca plate.

Components: 4385 words, 7 figures, 1 table, 1 animation.

Keywords: ambient noise; western United States.

Index Terms: 7255 Seismology: Surface waves and free oscillations; 7205 Seismology: Continental crust (1219); 9350 Geographic Location: North America.

Received 10 April 2007; **Revised** 5 June 2007; **Accepted** 19 June 2007; **Published** 21 August 2007.

Moschetti, M. P., M. H. Ritzwoller, and N. M. Shapiro (2007), Surface wave tomography of the western United States from ambient seismic noise: Rayleigh wave group velocity maps, *Geochem. Geophys. Geosyst.*, *8*, Q08010, doi:10.1029/2007GC001655.

1. Introduction

[2] Ambient noise surface wave tomography has been shown to produce accurate surface wave dispersion maps on multiple spatial scales over a broad period band [e.g., *Sabra et al.*, 2005; *Shapiro et al.*, 2005; *Lin et al.*, 2006, 2007; *Yang et al.*, 2007; *Yao et al.*, 2006]. In particular, the technique provides short period surface waves along interstation paths, which are inaccessible from earthquake tomography. Because earthquakes are primarily limited to plate margins and tectonically active regions, the tomography of aseismic regions requires the observation of teleseisms or the use of active sources. The long paths traveled by teleseism-generated waves preferentially attenuate

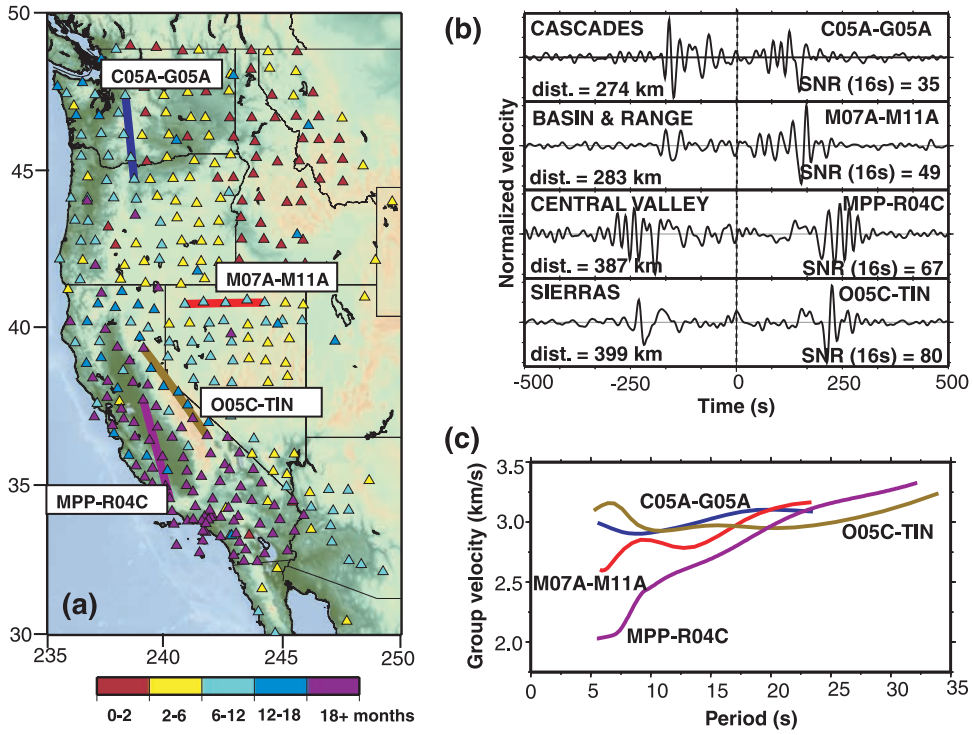

Figure 1. (a) Station locations used in this study, color coded by the time series length. Interstation paths for the measurements shown in Figures 1b and 1c are indicated. (b) Full, broadband cross-correlation waveforms from four receiver pairs. The waveforms result from time stacks of 3.4, 2.1, 17.5, and 13.6 months of data, respectively. (c) The dispersion curves are for the station-pairs labeled from the waveforms in Figure 1b.

and scatter shorter period surface waves, leading to weak constraints on crustal structures. In addition, the azimuthal distribution of paths from earthquakes is restricted by earthquakes. In contrast with traditional earthquake tomography, ambient noise tomography is limited primarily by the number and density of interstation paths.

[3] Investigation of crustal structure over broad expanses of the western US would benefit from short period dispersion maps. While the western US is tectonically active and parts are seismogenic, the larger magnitude regional earthquakes ($M_s > 5$) required for short period surface wave analysis are relatively infrequent and are primarily located in Southern California, off the Pacific Northwest coast, and along the Wasatch Front. The geographical distribution of epicenters is insufficient to produce high-resolution surface wave maps across most of the western US. Some surface wave analyses in southern California have made use of teleseismic events [e.g., *Tanimoto and Prindle Sheldrake*, 2002; *Yang and Forsyth*, 2006] to provide constraints on the mantle and ambient noise [*Sabra et al.*, 2005; *Shapiro et al.*, 2005] to constrain crustal structures. No surface wave studies, to the authors' knowledge, have presented results on the scale with the resolution presented here, however.

[4] Until recently, large regions of the western US were poorly instrumented, and the resolution of dispersion maps was greatly limited. Previous ambient noise tomography studies made use of data from permanent regional and national networks, particularly in southern California. A small number of highly instrumented regions have existed to provide dense station coverage on a local scale, but until recently, a widely distributed network with the dense station spacings needed to produce high-resolution images of the western United States did not exist.

[5] The emerging EarthScope USArray Transportable Array (TA) provides a nearly ideal network for the application of ambient noise surface wave tomography. Station coverage for the study region and period band is presented in Figure 1a. Station density is approximately uniform across the network, and excellent spatial and azimuthal coverage emerges from interstation paths. Average station spacing is approximately 70 kilometers, and once

built-out, more than 400 stations will be deployed simultaneously. Installation of the first TA stations occurred in 2004, and the network has been expanding across the western United States ever since.

[6] We make use here of ambient noise measurements from TA stations to generate high-resolution group velocity maps of the western United States. The study examines the resolution and group velocity maps produced for the western United States from a data set obtained from October 2004 through January 2007. During this period, the TA expanded to cover California, Oregon, Washington, most of Nevada and Idaho, and western Utah, Montana, and Arizona.

2. Methods and Data Processing

[7] Ambient noise data processing involves the cross-correlation of long time-sequences of ambient noise to extract estimated Green's functions. The dispersion characteristics of the estimated Green's functions provide information about the interstation wave propagation and hence about seismic velocities in the crust and uppermost mantle. We process seismic records from the TA and several regional networks within the western US region with the following coordinate boundaries: 30° to 50° North latitude, and 126° to 110° West longitude. By restricting data processing to vertical-component waveforms within the 5- to 50-s period band, we recover only Rayleigh wave arrivals.

[8] Our temporal normalization, spectral prewhitening, cross-correlation, and stacking procedures closely follow the methodology described by *Bensen et al.* [2007]. Cross-correlation waveforms possess signals at both positive (causal) and negative (acausal) correlation lag times, corresponding to waves propagating in opposite directions between the stations. Because of the seasonal variation in the amplitude and spectral content of these signals, we average the causal and acausal signals to yield the "symmetric-signal", which is used in all subsequent processing.

[9] Group velocity dispersion measurements are obtained using a frequency-time analysis (FTAN) [e.g., *Ritzwoller and Levshin*, 1998], but in automated form as described by *Bensen et al.* [2007]. *Bensen et al.* [2007] also promote a data selection criterion based on estimating uncertainties defined from the variation in seasonally averaged dispersion curves. This method, however, requires records of at least one year in duration, which are not available for all of the TA stations. Our selection of dispersion curves, therefore, differs slightly from theirs because the size of our data set grows over time. Instead, we use the signal-to-noise ratio (SNR) as a proxy for uncertainty and select group velocity measurements on the basis of two criteria. (1) The maximum period accepted from individual dispersion curves depends on the interstation distance, with three wavelengths taken as the minimum interstation spacing to accept a measurement. (2) Each group velocity measurement must derive from a cross-correlogram that exceeds a spectral SNR of 20. Because of the absence of meaningful uncertainty estimates, we use a higher SNR threshold than advocated by Bensen et al.

[10] Tomography proceeds in two steps on a half-degree-by-half-degree grid to generate group velocity maps. In the first step of tomography, we generate an overly smoothed map at each period which is used to identify and reject traveltime residual outliers. The standard deviation of traveltime eresiduals in four distance bins is computed, and measurements with time residuals greater than three standard deviations from the mean are rejected. The remaining measurements are used in the second step of tomography to yield the final resolution and group velocity maps based on the tomographic method of *Barmin et al.* [2001]. This method uses Gaussian-shaped sensitivity kernels centered on the great-circle between the stations. Our simulations show that this simple approximation to the sensitivity kernels appears to be sufficient at the periods and interstation distances of this study, but clearly more work is needed to understand wave propagation at the short period end of the study. We fit a 2-D symmetric Gaussian function to the resolution surface at each node and report resolution as twice the estimated standard deviation. Future investigations into the contribution from higher-order wave propagation effects, such as off-great-circle propagation, more accurate finite-frequency sensitivity kernels, and multipathing, are appropriate, but the resulting modifications to the dispersion maps are expected to be relatively small [*Ritzwoller et al.*, 2002].

3. Results

[11] Continuous ambient noise records were collected from October 2004 through January 2007. During the study period, the number of stations increased from 93 to 340 as the TA grew. The expansion of the TA to the north and east during

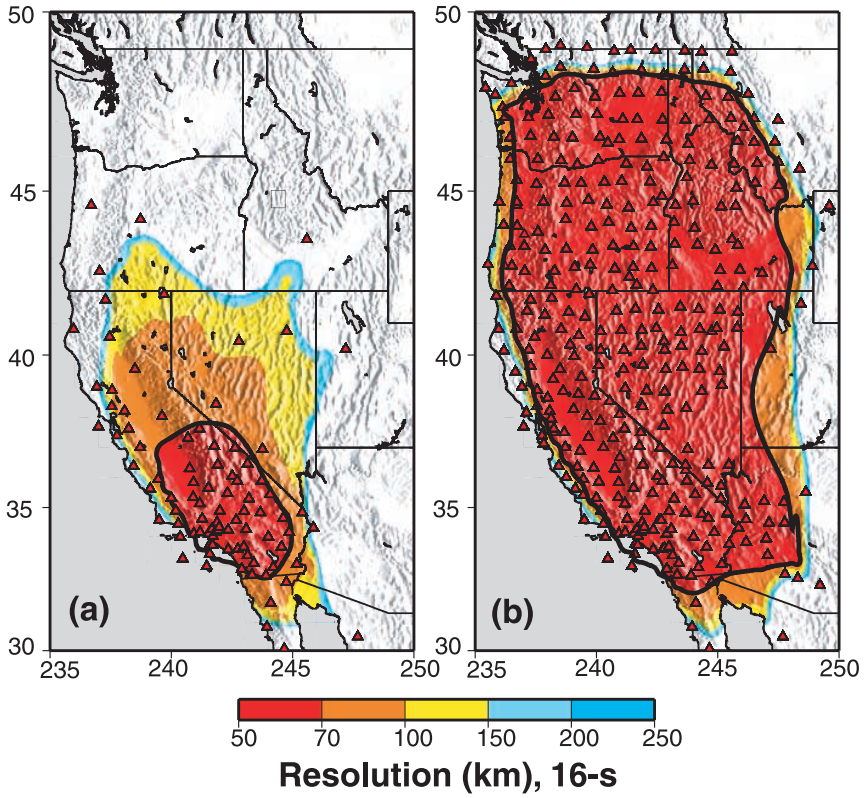

Figure 2. Comparison of the 16-s period resolution maps for data from (a) October 2004 and (b) October 2004 through January 2007. The 70 km resolution contour is drawn for reference in both panels, and stations used in each period are plotted as red triangles.

this study period is reflected in the considerable variability in the time series lengths (Figure 1a). Cross-correlation of all contemporaneous continuous records produces 55108 cross-correlograms. This number is in contrast with the 4005 cross-correlograms from the initial October 2004 data set.

[12] Examples of the full cross-correlation waveforms are presented in Figure 1b. The four waveforms are from paths in the Cascades, the Basin and Range, the Great Valley of California, and the Sierra Nevada and result from time stacks of 3.4, 2.1, 17.5, and 13.6 months of data, respectively. Asymmetry in the cross-correlations results from an inhomogeneous distribution of ambient noise sources [*Stehly et al.*, 2006]. Using the Cascades waveform in Figure 1b as an example (C05A is the northern station), the positive lag represents the wave propagation from station C05A to station G05A, and the negative lag represents the reverse propagation. The larger amplitude of the negative lag suggests that the dominant noise source originates from the south during the 3.4 months of joint operation presented here. Aspects of ambient noise sources derived from long range correlation properties have been characterized by several investigators [e.g., *Shapiro et al.*, 2006; *Stehly et al.*, 2006].

[13] Some insight into local crustal structure may be gained from the example dispersion curves in Figure 1c. The curves from the Cascades and the Sierras show fast short period group velocities, suggesting an absence of, or thin, sedimentary deposits. The shallow slope of the Sierran dispersion curve suggests a thick crust along the propagation path. The very slow short period group velocities from the Great Valley suggest thick sedimentary deposits; the large slope results from the increasing sensitivity to basement material with increasing wave period. The surface deposits in the Basin and Range appear to be intermediate in group velocity to the crystalline rocks of the Sierras and Cascades and the sediments of the Great Valley.

[14] Between 21% (40-s) and 58% (16-s) of the original cross-correlograms passed the data selection criteria for use in the tomographic inversions. The great majority of the rejected measurements

Table 1. Number of Paths Rejected Prior to Group Velocity Tomography at 8-, 16-, 24-, 30-, and 40-s Periods

	Period				
	8-s	16-s	24-s	30-s	40-s
Total waveforms	55108	55108	55108	55108	55108
SNR rejections (SNR < 20)	22101	17864	20536	22830	25386
Distance rejections	964	3525	7333	10724	16777
FTAN measurement failure	6634	1037	438	413	407
Time residual rejection	1423	1047	692	642	725
Remaining measurements	23986	31635	26109	20499	11813

(74% – 97%) result from the high SNR threshold and the interstation distance criterion. Table 1 summarizes the measurement rejections at each step of data processing and selection.

[15] Resolution maps are constructed at 8-, 16-, 24-, 30-, and 40-s periods. A comparison of the 16-s period resolution map from October 2004 with that from the January 2007 data stack is presented in Figure 2. The contour line designates a resolution of 70 km and encloses the region of high resolution. Between October 2004 and January 2007, this region increased in size by factors of 8.7 (8-s), 7.9 (16-s), and 12.4 (24-s). Too few paths were available at 30- and 40-s periods to generate group velocity maps at those periods from the October 2004 data set. The resolution across the western US is comparable to the interstation spacing from the TA.

[16] Velocity anomalies in the group velocity maps are observed to be stable with respect to increasing time series lengths. Figure 3 presents the tomography results at 16-s period for time series lengths of 1, 6, 18, and 28 months. The black contour encircles the region of high resolution in each figure frame. The dominant features in the high-resolution region of the group velocity map produced from the 1-month time series include high-velocity anomalies for the Sierra Nevada and Peninsular Ranges and low-velocity anomalies in the southern Great Valley and Coast Ranges. These features remain stable in the group velocity maps as the Transportable Array grows to the north

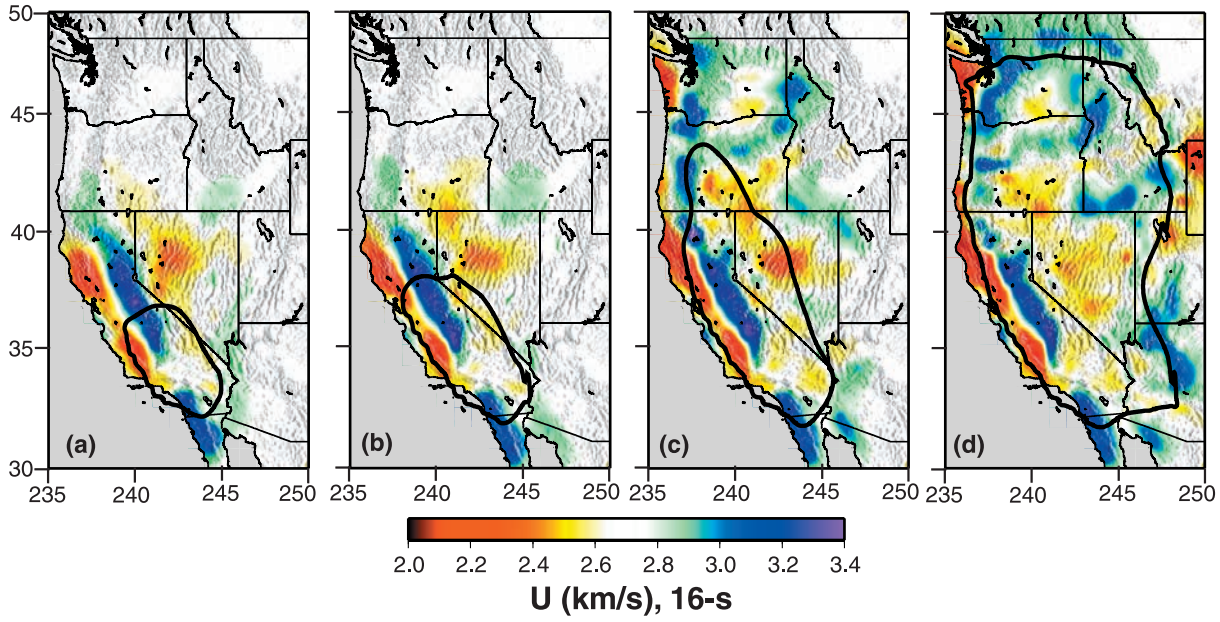

Figure 3. Growth of the 16-s Rayleigh wave group velocity map with increasing time series length as the Transportable Array expanded: (a) 1 month (October 2004), (b) 6 months (October 2004 to March 2005), (c) 18 months (October 2004 to March 2006), and (d) 28 months (October 2004 to January 2007). The 70 km resolution contour is drawn for reference in all panels.

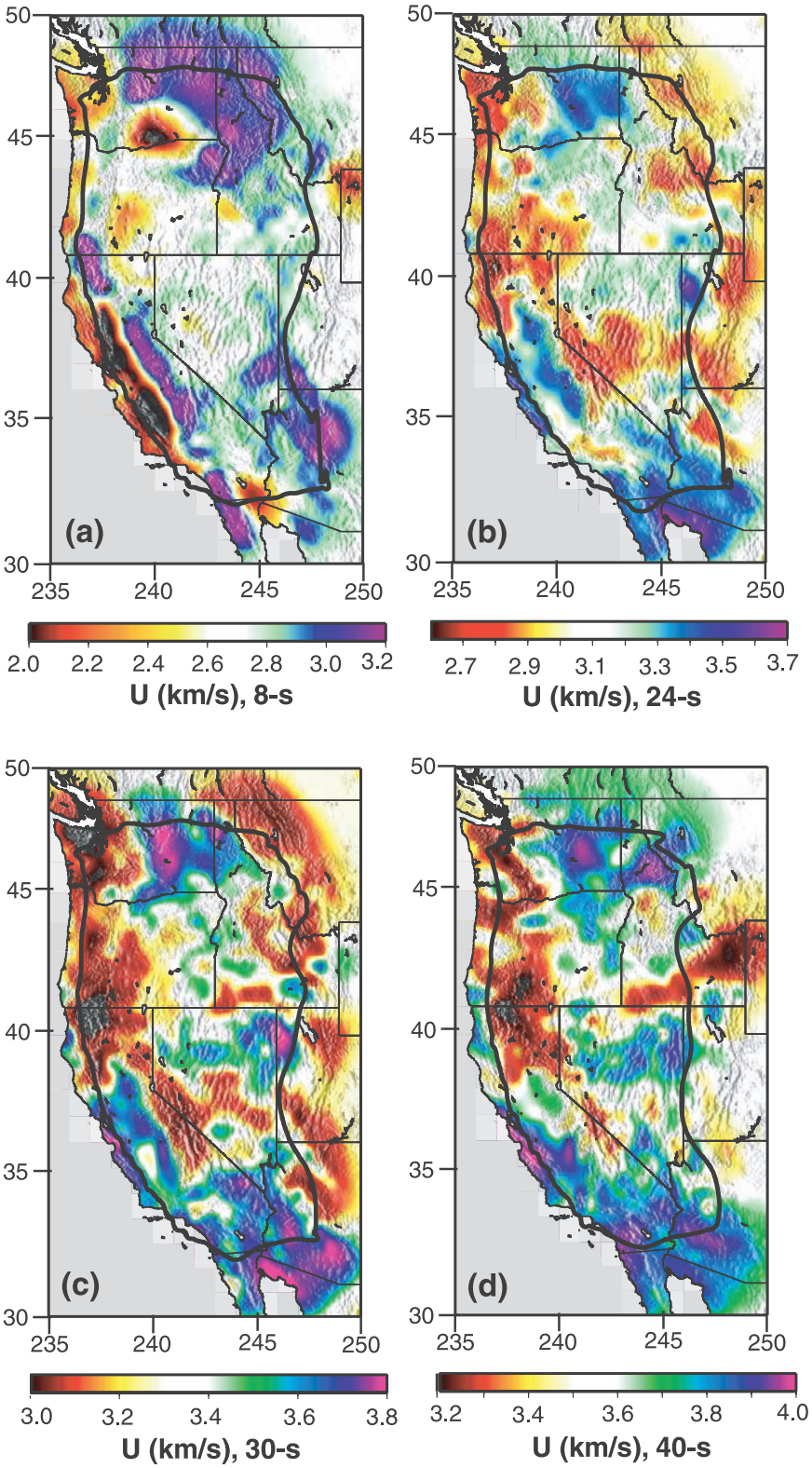

Figure 4. Rayleigh wave group velocity maps: (a) 8-s period, (b) 24-s period, (c) 30-s period, and (d) 40-s period. The 70 km resolution contour is drawn for reference in all panels.

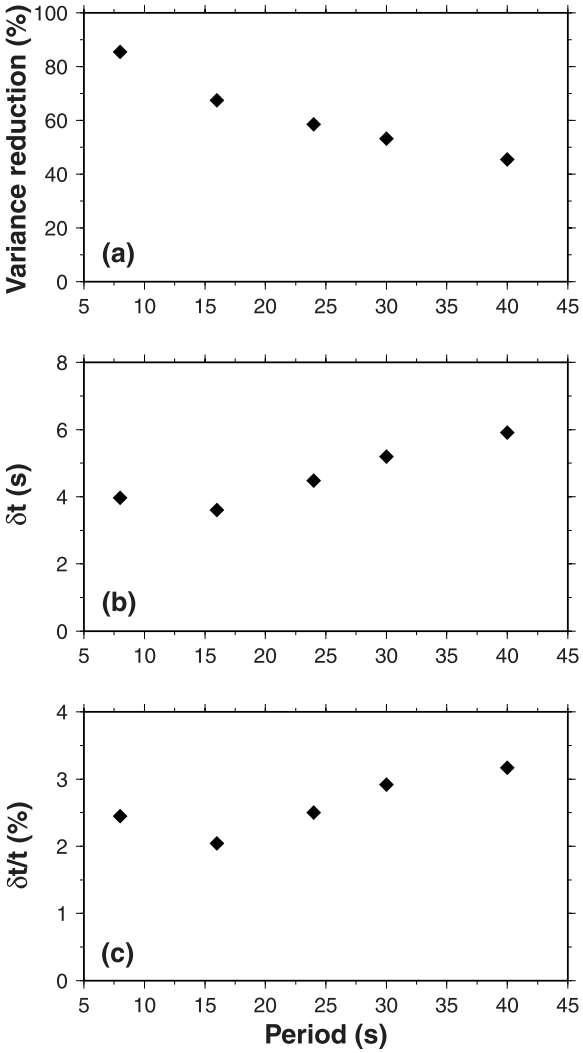

Figure 5. (a) Misfit is presented as the reduction of variance by the estimated group velocity maps compared to the average group velocity across each map at 8-, 16-, 24-, 30-, and 40-s periods. (b) RMS traveltime misfit at 8-, 16-, 24-, 30-, and 40-s periods. (c) RMS traveltime misfit normalized by total traveltime at 8-, 16-, 24-, 30-, and 40-s periods.

and east, despite an increase in time series lengths for southern California stations up to more than two years in duration and the introduction of long paths to stations outside southern California. Over-all, during the period of this study, the number of paths increased from 1741 to 31635 at 16-s period. With increasing time series lengths and the growth of the TA, the resolution of the features in southern California improves and small changes in amplitude are observed. While the duration of time series lengths for TA stations is limited by installation times, longer time series are preferable both for the equilibration of the velocity anomaly amplitudes and to determine uncertainties from temporal variability.

[17] The stability of the velocity anomalies is also observed in an animation of the 16-s Rayleigh was tomography map between October 2004 and January 2007 (see dynamic content Animation 1). Each frame in the animation differs by the addition of one month of data. The frames at 1, 6, 18, and 28 months correspond to the respective frames in Figure 3. As observed in Figure 3, velocity anomalies at 16-s period become relatively stable with one month of data. The addition of stations external to the inverted region increases the area of the tomographic maps and the coverage of the high-resolution region, with only small adjustments to the velocity anomalies.

[18] The 8-, 16-, 24-, 30- and 40-s periods Rayleigh wave group velocity maps are presented in Figures 3 and 4. The 70 km resolution contour provides an approximate boundary for the high-resolution tomography. However, the larger-scale features directly outside of the contour are probably meaningful. The poor resolution at the edge of the continent results from the absence of paths crossing the coastline.

[19] The reduction in variance produced by the 28-month maps at each period relative to the average group velocity across each map and the root-mean-squared traveltime and normalized traveltime are plotted in Figure 5. Variance reduction ranges between 45% and 85% and is observed to decrease with increasing period. This trend results from the smaller amplitude traveltime anomalies and the longer average interstation

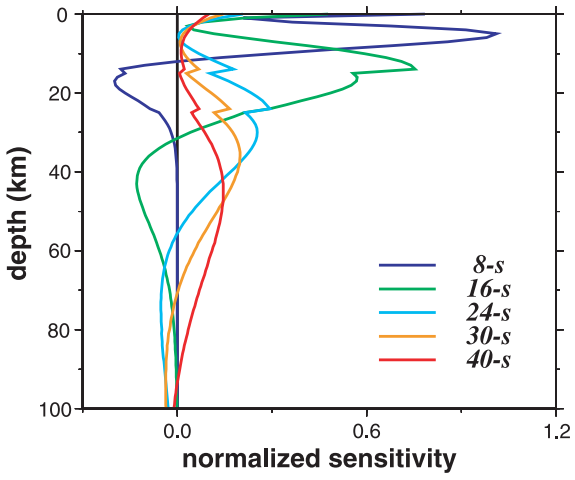

Figure 6. Depth sensitivity of 8-, 16-, 24-, 30-, and 40-s Rayleigh group wave periods.

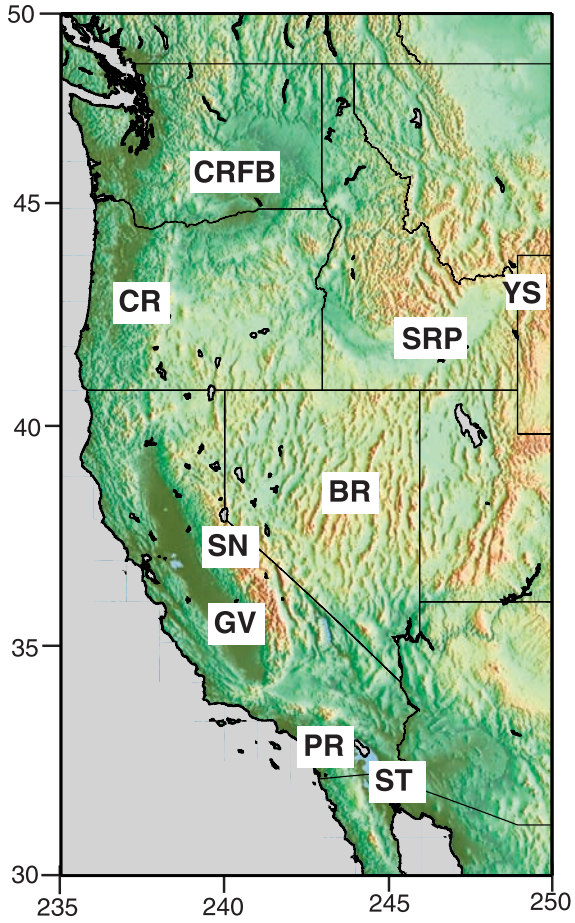

Figure 7. Geological features of the western United States. Features correlated with velocity anomalies in the Rayleigh wave group velocity maps include the Basin and Range province (BR), Cascade Range (CR), Columbia River Flood Basalts (CRFB), Great Valley (GV), Peninsular Range (PR), Salton Trough (ST), Sierra Nevada Range (SN), Snake River Plain (SRP), and Yellowstone (YS).

distances at longer periods. Traveltime misfits at 8-, 16-, 24-, 30- and 40-s periods are 4.0, 3.6, 4.5, 5.2, and 5.9 s, respectively. Because of the imposition of a three-wavelength criterion for data selection, average path lengths between 8 and 40 s periods increase from 578.4 to 728.4 km. Normalizing the traveltime misfits by total traveltime results in misfits between 2 and 3.2%, and misfits to the model are observed to be approximately equal for all periods.

4. Discussion

[20] *Shapiro et al.* [2005] first showed that the features appearing in the group velocity maps that result from ambient noise tomography correlate well qualitatively with known geological structures. Here, we note similar qualitative correlations across a much larger area with more diverse geological structures and tectonic history. A more definitive determination of structural causes, however, must await inversion for 3-D structure. To guide interpretation, the shear velocity radial sensitivity kernels for Rayleigh group velocity at periods of 8-, 16-, 24-, 30- and 40-s are plotted in Figure 6. The model used to construct the kernels is PREM, in which the ocean has been replaced with a sedimentary layer. Discontinuities in the kernels result from the layered nature of the velocity model. Figure 7 identifies the locations of some of the dominant geological features observed in the Rayleigh wave group velocity maps and referred to below.

[21] The group velocity maps at short periods display features that derive predominantly from shallow lateral compositional variations between the crystalline cores of mountain ranges, sedimentary basins, and extended volcanic provinces. At longer periods, there is increasing sensitivity to crustal thickness (fast denoting thin crust, slow denoting thick crust) as well as deep crustal and uppermost mantle temperature anomalies.

[22] Mountain ranges typically present as fast short period group velocity anomalies due to crystalline rocks extending nearly to the surface. Variations in crustal composition and thickness create distinctive patterns with period for each structural feature. For example, the Sierra Nevada and Peninsular Ranges are associated with high-velocity anomalies through the 24-s period maps, with lower-velocity anomalies at longer periods. In contrast, the Cascades present high velocities only to about 16-s period. These differences are reflective of differences in crustal thickness and velocities.

[23] Sedimentary basins appear as low-velocity anomalies at short periods due to the slow shear velocities of sediments. However, basins often overlie thin crust and, therefore, at longer periods may appear as high-velocity anomalies. The most prominent sedimentary basin in the western US is the Great Valley of California where low-velocity anomalies are observed to 16-s period. At short periods, the deep sediments result in uniform slow anomalies across the valley. As periods increase and wave sensitivity deepens, there is a clear separation into the San Joaquin Basin to the south and the Sacramento Basin to the north. The anomalies increase in velocity with period as the waves become sensitive to basement material.

The Salton Trough also presents slow velocity anomalies at short periods, but with intermediate speeds at 16-s and high velocities at 24-s period. This is consistent with a rift basin located at the boundary between the North American and Pacific Plates with very thin crust. Similar short period anomalies appear in the Columbia River Basin, but are more difficult to interpret.

[24] Volcanic features also manifest on the observed group velocity maps. For example, Columbia River flood basalts correlate with fast anomalies at all periods up to the 40-s period map. Of particular note, the Snake River Plain in southern Idaho outlines a high-velocity anomaly on the 16-s map, presumably caused by the middle to lower crust beneath this feature being compositionally distinct from surroundings. Although it is hard to see from Figure 3d, the high-speed anomalies gradually slow toward Yellowstone to the east. At longer periods, however, the Snake River Plain is underlain by slow anomalies, again that slow to the east toward Yellowstone. These low-velocity anomalies are probably thermal in original, resulting from relatively warm lower crust and uppermost mantle and temperatures that increase toward Yellowstone. Yellowstone, although outside the current high-resolution region, is slow at all periods.

[25] Four other correlations are worth mentioning. (1) A broad region of higher-velocity anomalies at intermediate and long periods from southwestern Arizona to northern Baja California and through the Salton Trough region is likely due to relatively thin crust in the region. (2) Slow anomalies are observed at intermediate to long periods across much of western to central Oregon and Washington, and are probably reflective of warm temperatures in the crust and uppermost mantle in the mantle wedge overlying the subducting Juan de Fuca Plate. High volatile content may also depress shear velocities in this region. Since the resolution of the maps deteriorates at the coastlines, ambient noise studies of this region would greatly benefit from the emplacement of ocean-bottom seismometers. The current PASSCAL deployments in the region (Oregon Array for Teleseismic Study and Cascadia Array for EarthScope) will provide important results on the upper mantle structure of this region. (3) The Basin and Range Province in Nevada displays fast anomalies in the north and slower anomalies in the south and may reflect lower crustal temperatures and perhaps thinner crust in the north. (4) On the 40-s map, a north-south transition from high to low velocity occurs near Cape Mendocino at the hypothesized southern edge of the Juan de Fuca Plate. Further investigation is warranted into evidence for potential upwellings or corner flow [e.g., *Levin et al.*, 2002].

5. Conclusions

[26] Ambient noise surface wave tomography has been applied to emerging data from the EarthScope USArray Transportable Array (TA) in the western United States to produce high-resolution group velocity maps. Using data collected between October 2004 and January 2007, we generate cross-correlations between all receiver pairs and measure group velocity dispersion characteristics. Rayleigh wave group dispersion curve selection at each period produces between 11000 and 32000 paths for inversion for group velocity maps at 8-, 16-, 24-, 30-, and 40-s periods. The resulting group velocity anomalies are well-correlated with known geological features. The expansion of the TA during the twenty-eight month study period resulted in a significant increase in the spatial extent of the high-resolution parts of these maps. Resolution across much of the western US is equal to the average interstation spacing (~70 km). Continually lengthening time series from the growth of the TA will produce more reliable measurements and the extraction of increasingly accurate tomographic features in future maps.

[27] The application of ambient noise tomography to continuous records from the TA presents unique information about the crust and upper mantle of the western US. Rayleigh wave group velocity maps show strong anomalies correlated with the Sierra Nevada, Peninsular, and Cascade Ranges, the Great Valley, Salton Trough, and Columbia Basins, the Columbia flood basalts, the Snake River Plain track and the Basin-and-Range province. The middle- to lower-crustal slow anomalies observed at Yellowstone and the southern extent of the subducting Juan de Fuca plate are suggestive of crustal heating or the presence of volatiles associated with mantle upwelling in those regions. The technique produces higher-resolution Rayleigh wave group velocity maps within the TA footprint than have been possible using earthquakes. Measurements below 10-s period are readily obtained. Poor network coverage at the edges of the array and coastal margins limit the resolution in those regions. Expansion of the TA will continue to increase the spatial extent and improve the resolution at the eastern edges of the

group velocity maps presented here. Application of the method to isotropic phase velocities and Love waves, azimuthal anisotropy, and use of the resulting dispersion maps to infer the 3-D distribution of shear wave velocities in the crust and uppermost mantle are natural extensions of this study and are currently underway.

Acknowledgments

[28] The data used in this research were obtained from the IRIS Data Management Center. This research was supported by NSF grant EAR-0450082. M.P.M. acknowledges a National Defense Science and Engineering Graduate Fellowship from the American Society for Engineering Education. All figures were created using GMT [*Wessel and Smith*, 1998]. The authors thank Richard Allen and an anonymous reviewer and associate editor James Gaherty for their helpful comments.

References

Barmin, M. P., M. H. Ritzwoller, and A. L. Levshin (2001), A fast and reliable method for surface wave tomography, *Pure Appl. Geophys.*, *158*, 1351–1375.

Bensen, G. D., M. H. Ritzwoller, M. P. Barmin, A. L. Levshin, F.-C. Lin, M. P. Moschetti, N. M. Shapiro, and Y. Yang (2007), Processing seismic ambient noise data to obtain reliable broad-band surface wave dispersion measurements, *Geophys. J. Int.*, doi:10.1111/j.1365-246X.2007.03374.x.

Levin, V., N. M. Shapiro, J. Park, and M. H. Ritzwoller (2002), Seismic evidence for catastrophic slab loss beneath Kamchatka, *Nature*, *418*, 763–767.

Lin, F.-C., M. H. Ritzwoller, and N. M. Shapiro (2006), Is ambient noise tomography across ocean basins possible?, *Geophys. Res. Lett.*, *33*, L14304, doi:10.1029/2006GL026610.

Lin, F., M. H. Ritzwoller, J. Townend, S. Bannister, and M. K. Savage (2007), Ambient noise Rayleigh wave tomography of New Zealand, *Geophys. J. Int.*, doi:10.1111/j.1365-246X.2007.03414.x.

Ritzwoller, M. H., and A. L. Levshin (1998), Surface wave tomography of Eurasia: Group velocities, *J. Geophys. Res.*, *103*, 4839–4878.

Ritzwoller, M. H., N. M. Shapiro, M. P. Barmin, and A. L. Levshin (2002), Global surface wave diffraction tomography, *J. Geophys. Res.*, *107*(B12), 2335, doi:10.1029/2002JB001777.

Sabra, K. G., P. Gerstoft, P. Roux, W. A. Kuperman, and M. C. Fehler (2005), Surface wave tomography from microseisms in southern California, *Geophys. Res. Lett.*, *32*, L14311, doi:10.1029/2005GL023155.

Shapiro, N. M., M. Campillo, L. Stehly, and M. H. Ritzwoller (2005), High resolution surface wave tomography from ambient seismic noise, *Science*, *307*, 1615–1618.

Shapiro, N. M., M. H. Ritzwoller, and G. D. Bensen (2006), Source location of the 26 sec microseism from cross-correlations of ambient seismic noise, *Geophys. Res. Lett.*, *33*, L18310, doi:10.1029/2006GL027010.

Stehly, L., M. Campillo, and N. M. Shapiro (2006), A study of the seismic noise from its long-range correlation properties, *J. Geophys. Res.*, *111*, B10306, doi:10.1029/2005JB004237.

Tanimoto, T., and K. Prindle Sheldrake (2002), Three-dimensional S-wave velocity structure in Southern California, *Geophys. Res. Lett.*, *29*(8), 1223, doi:10.1029/2001GL013486.

Wessel, P., and W. H. F. Smith (1998), New, improved version of the Generic Mapping Tools released, *Eos Trans. AGU*, *79*(47), 579.

Yang, Y., and D. W. Forsyth (2006), Rayleigh wave phase velocities, small-scale convection, and azimuthal anisotropy beneath southern California, *J. Geophys. Res.*, *111*, B07306, doi:10.1029/2005JB004180.

Yang, Y., M. H. Ritzwoller, A. L. Levshin, and N. M. Shapiro (2007), Ambient noise Rayleigh wave tomography across Europe, *Geophys. J. Int.*, *168*, 259–274.

Yao, H., R. D. van der Hilst, and M. V. de Hoop (2006), Surface-wave tomography in SE Tibet from ambient noise and two-station analysis: I. — Phase velocity maps, *Geophys. J. Int.*, *166*, 732–744.